FINAL REPORT

MECHANICAL BEHAVIOR OF POLYCRYSTALLINE CERAMICS: BRITTLE FRACTURE OF SiC-Si_3N_4 MATERIALS

BY

MARTIN H. LEIPOLD
CAWAS M. KAPADIA
ANANT H. KELKAR

DEPARTMENT OF METALLURGICAL ENGINEERING AND MATERIALS SCIENCE

UKY TR84-74-MET19
APRIL 1974

SUBMITTED TO:

NASA LEWIS RESEARCH CENTER
CLEVELAND, OHIO

NASA GRANT NGL 18-001-042

UNIVERSITY OF KENTUCKY
UNITED WE STAND DIVIDED WE FALL
18 65

ENGINEERING UK

For additional copies or information address correspondence to:
ORES Publications
College of Engineering
University of Kentucky
Lexington, Kentucky 40506

A PUBLICATION OF THE OFFICE OF RESEARCH AND ENGINEERING SERVICES

UKY TR84–74–MET19
AUGUST 1974

FINAL REPORT

MECHANICAL BEHAVIOR OF POLYCRYSTALLINE CERAMICS: BRITTLE FRACTURE OF SiC–Si_3N_4 MATERIALS

by

Martin H. Leipold
Associate Professor of
Materials Science

Cawas M. Kapadia
Research Assistant

Anant H. Kelkar
Research Assistant

College of Engineering
University of Kentucky

Submitted to

The Lewis Research Center of
The National Aeronautics and Space Administration
Cleveland, Ohio

as part of

NASA Grant NGL 18-001-042

April 1, 1974

CONTENTS

LIST OF FIGURES

LIST OF TABLES

I. INTRODUCTION

This report represents the conclusion of a five-year research effort investigating various properties of ceramic materials. The research represents two main areas of investigation. The first involved magnesium oxide and the role of anion impurities, while the second was directed toward slow crack growth in silicon nitride-silicon carbide ceramics. The oxide program involved development of fabrication techniques for anion doped materials and evaluation of the role of these anions in the hot pressing response, grain boundary diffusion of nickel doped material, grain boundary microhardness, and grain growth. Each of these aspects represents a separate subheading, and results are reported essentially independently.

The carbide-nitride work employed commercial materials and the research involved evaluation of a recently reported technique for study of slow crack growth and the development of data for these commercial materials.

Four prior Annual Reports have been prepared as a part of this program, as well as a number of publications in the open literature and oral presentations. The titles and sources are listed in Appendix I. Each section of this report lists the reports and presentations, providing information pertaining to this subject, including publications in preparation but not yet available. Additionally, each section includes new results and interpretations not previously reported in Annual Reports.

The authors would like to acknowledge the assistance of J. J. Brawley, D. B. Duff, G. D. Chambliss, and M. A. Shakel in the laboratory.

II. OXIDE STUDIES

The oxide research was begun with the inception of this research program and has received decreasing emphasis with time, consequently, the major portions of the work have been completed, analyzed and reported in the open literature. Pertinent reports for each subdivision are listed under that topic. In addition, new results and interpretation are included.

A. Fabrication

The importance of anion impurities on the hot pressing behavior is completely described in Reports 1, 7 and 8 in the Appendix. No additional detail is available.

B. Grain Boundary Microhardness

The results here were given in a preliminary manner in Reports 7 and 11 in the Appendix. Additional effort has been made to more clearly substantiate the lack of any measurable effect of anions on microhardness. The additional analysis has continued to indicate lack of any effect. It must be concluded, therefore, that with the experimental precision of these tests, anions do not result in grain boundary hardness changes.

C. Grain Growth

The results of this work have largely been published in Reports 2, 3, 4, 5, 6, 9, 10 and 12 in the Appendix. However, because of the large effort and because of the general conclusions that have not been given in a previous report, they are presented here.

For undoped MgO, an activation energy of 65 ± 2 kcal per gram-mole was obtained for grain growth in high purity, theoretically dense material. Further, squared (n = 2) grain growth kinetics corresponding to boundary control were observed. However, such high purity material in the presence of only 0.5% porosity gave pore inhibited grain growth.

For the doped MgO, the influence of the anions depended on the porosity levels of the material. For less dense MgO (>1% porosity), kinetics were pore-controlled and the effect of the anions, if any, were not immediately obvious. Influence of the anions with respect to pore removal and boundary migration will be apparent only at very low porosity levels. For the dense material (porosity <1%), a distinct enhancement in growth rates existed for OH^-, F^-, and Cl^-, while rates for S^{2-} correspond to those of undoped Fisher MgO.

At both 1300 and 1500°C, the promoter anions (OH^-, F^-, and Cl^-) in the dense material are equivalent to each other, especially at large anneal times. The grain sizes for these anions are distinctly larger than for S^{2-} or the undoped material.

Hence, in comparison, the effect of the anions on grain growth is in the order $OH^- = F^- > Cl^- > S^{2-}$. Anion impurities were shown to be deleterious to densification of MgO by hot-pressing in the order $S^{2-} > Cl^- > F^- > OH^-$. Hence, any effect of these anions on grain growth can be related directly to their effect on densification.

In addition, the large quantity of data developed in the research clearly indicated the complex time-dependent changes in the kinetics of grain growth occurring in these ceramics. For example, in several cases, at least three types of kinetics were observed, corresponding to, first, uninhibited growth (n = 2); next, limiting growth (n = ∞); and finally, impurity controlled (n = 3). The existence of plateaus

in grain size ($n = \infty$) as a transition in behavior has apparently not been specifically reported previously.

D. Grain Boundary Diffusion

The initial results in Reports 9 and 13 in the Appendix have been extended over a wider temperature range (1000 - 1500°C) and have been analyzed for grain boundary diffusion of nickel. Since the results have not been completely prepared for publication in the open literature, they are given here for the sake of completeness. Pertinent background literature experimental details are given first.

Diffusion on N_i^{2+} in single MgO crystals has been reported in the literature. For cleaved MgO crystals, Zaplatynsky (Ref. 1) obtained an activation energy of 36 kcal per mole in the temperature range of 1200 to 1450°C. Wuensch and Vasilos (Ref. 2), working in the temperature range 1000 - 1850°C, obtained activation energy for N_i^{2+} diffusion as 48 kcal per mole. Further, the transport rates were not significantly dependent on the impurity content or the dislocation densities. The relatively low dependence of diffusion rates on dislocation density was also observed in pipe diffusion studies (Ref. 3) for N_i^{2+} in MgO, where the diffusion along the dislocations was not appreciably enhanced.

Grain boundary diffusion of N_i^{2+} has been investigated in polycrystalline MgO and also in insulated grain boundaries in bicrystals of MgO. Results from diffusion couples, in which a surface was maintained at constant concentration during the diffusion annealing, indicate that the grain boundary diffusion is predominant in polycrystalline MgO at temperatures below 1700°C (Ref. 4). Grain boundary diffusion is considered to be an extrinsic process arising from impurity segregation and

precipitation at the grain boundaries. Grain boundary diffusion in MgO is not confined to a layer of atomic dimensions, but extends over a zone of the order of microns. Further, the activation energy for grain boundary diffusion of N_i^{2+} in MgO is between 23 and 46 kcal per mole (Ref. 4).

The procedures used in specimen preparation were straightforward. The MgO polycrystals were prepared by hot-pressing Fisher MgO powder mixed with the different anion dopants. The hot-pressing equipment and techniques are given in references 5 and 6. Table I gives the fabrication parameters of MgO specimens used for the diffusion anneals. To promote grain growth to get reasonably large sizes, these specimens were annealed at different temperatures for various lengths of time prior to the actual diffusion runs. The parameters for the grain growth reheats are given in Table II.

Diffusion couples were prepared by packing the doped MgO polycrystals in Baker Reagent Grade NiO powder in a 1/2 inch steel die and pressing at room temperature to approximately 5000 psi. The compacts were then placed in alumina crucibles and transferred to an electrical resistance furnace with SiC heating elements. The diffusion runs were made isothermally at temperatures ranging from 1000°C to 1500°C (at 100°C intervals) for approximately one week. To prevent shattering of the MgO specimens, the diffusion couples were very gradually removed from the furnace and air-cooled at the completion of the anneal. After most of the adhered NiO was removed, the specimens were cold mounted. A face which was at right angles to the MgO-NiO interface was metallographically polished, carbon coated in a vacuum evaporator, and subsequently used in an electron microprobe

Table I. Composition and Fabrication Parameters for Specimens for Diffusion Anneals.

Specimen No.	Initial Dopant At. %	Hot - Pressing Conditions			As pressed density gm/cm^3	As pressed bulk analysis At. %
		Max. Temp. C	Max. Press. Ksi.	Atmosphere*		
30	0.58% S^{2-}	960	20	V	3.55	0.03% S
110	3% F^-	1100	15	V	3.53	0.9% F
115	3% Cl^-	1100	15	V	3.56	0.06% Cl
120	3% OH^-	1100	15	V	3.54	
132	None	1000	15	A	3.56	None

* A = Argon; V = mechanical pump vacuum.

analyzer to determine the diffusion profiles*.

Briefly, the procedure was to make 220 μ long sweeps parallel to the specimen edge with a 12 μ wide beam. Sweeps were repeated after 12 μ displacements in a direction perpendicular to the specimen edge, until the nickel levels reached background.

Diffusion data were obtained using the relationship

$$C(x,t) = K\left(\frac{Dt}{\delta 2}\right)^{1/2} \exp\left(\frac{-4D}{\pi(\delta D')^2 t}\right)^{1/4} x$$

where C(x,t) is the atomic concentration of diffusion specie

x is depth (cm)

t is time (sec)

D is lattice diffusion constant** (cm^2/sec)

D' is the grain boundary diffusion constant (cm^2/sec), and

δ is the effective grain boundary width (cm)

This expression is used here because it may be simplified to linear plots of ln [concentration] versus penetration, and the data here were consistent with such a presentation. Sample plots are shown in Fig. 1. The diffusion constants were determined by computer, using a linear-least-squares fit. The interval over which the fit was determined was reduced until the standard deviation no longer decreased.

Activation plots were then made for each anion. Data for the undoped material are given in Figs. 2-6, and for all data in Table II. It is readily apparent that the values of diffusivity and the calculated activation energies and pre-exponentials differ

---

* Courtesy H. H. Stadelmaier, North Carolina State University, Raleigh.

** Data from Ref. 7: $D = 6.31 \times 10^{-6} \exp(-42800/RT)$.

Table II. Grain Boundary Diffusion Coefficients x Width For Ni^{+2} In Anion Doped Polycrystalline MgO

Temp. °C	Anion Dopant	G.D. x δ cm^3/sec	95% Confidence Limits (±)
1000	None	0.74×10^{-15}	$.14 \times 10^{-15}$
	Cl	1.43	.38
	F	1.52	.12
1100	None	1.6×10^{-15}	1.4×10^{-15}
	Cl	4.4	.78
	F	2.1	.80
	OH	4.2	.5
	S	5.7	3.7
1200	Cl	4.2×10^{-15}	1.2×10^{-15}
	F	3.0	1.4
	OH	7.5	1.5
	S	5.9	1.4
1300	None	7.6×10^{-14}	1.1×10^{-14}
	Cl	5.6	.51
	F	5.8	1.1
	OH	3.8	.59
	S	9.5	
1400	None	0.43×10^{-13}	$.038 \times 10^{-13}$
	Cl	0.95	.20
	F	3.3	.90
	OH	0.31	.03
	S	3.2	.20
1500	F	2×10^{-13}	$.59 \times 10^{-13}$
	OH	5.5	1.1
	S	4.2	.82

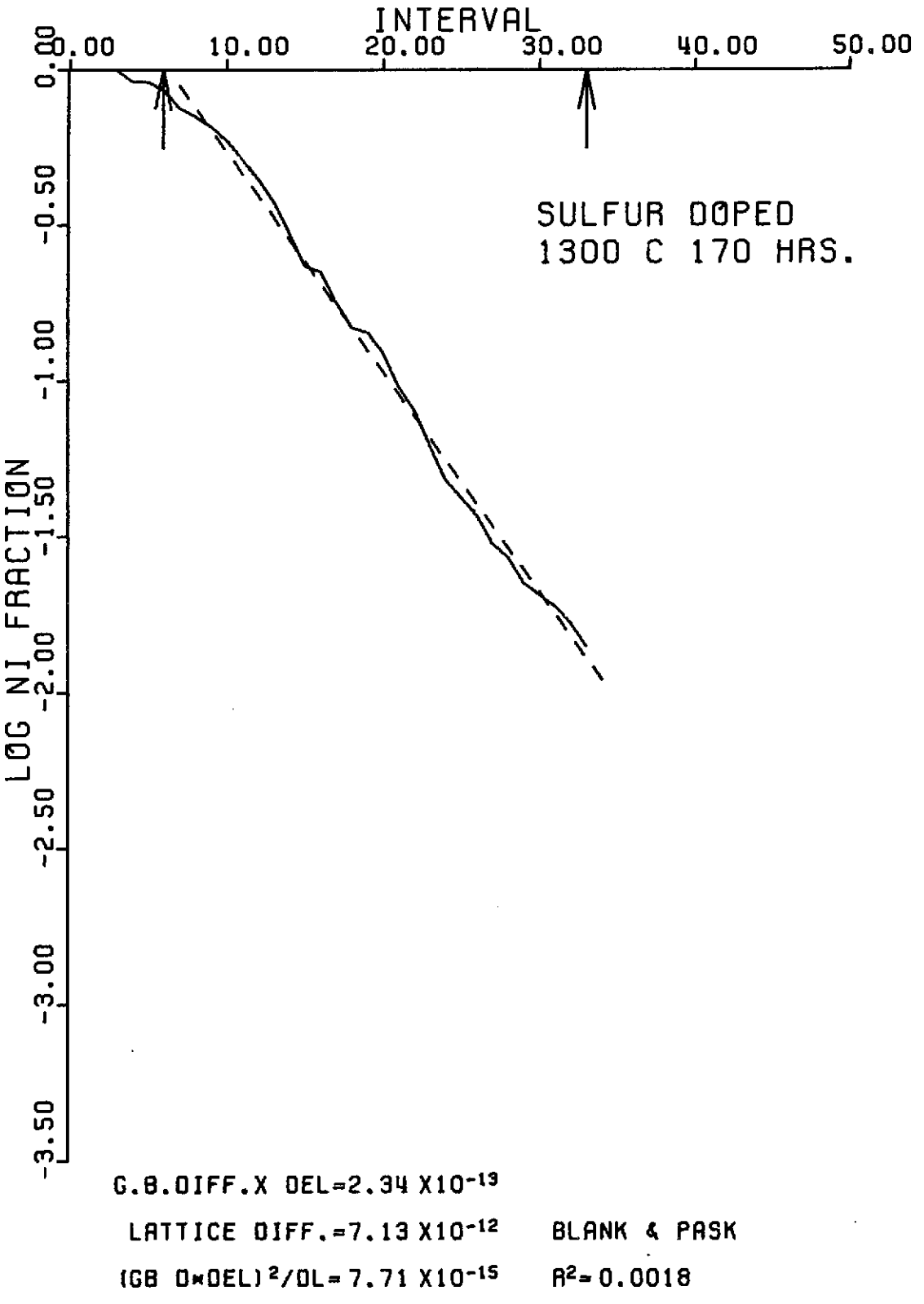

Fig. 1a. Diffusion profile for Ni^{2+} in sulfur doped MgO (R^2 is square of standard error)

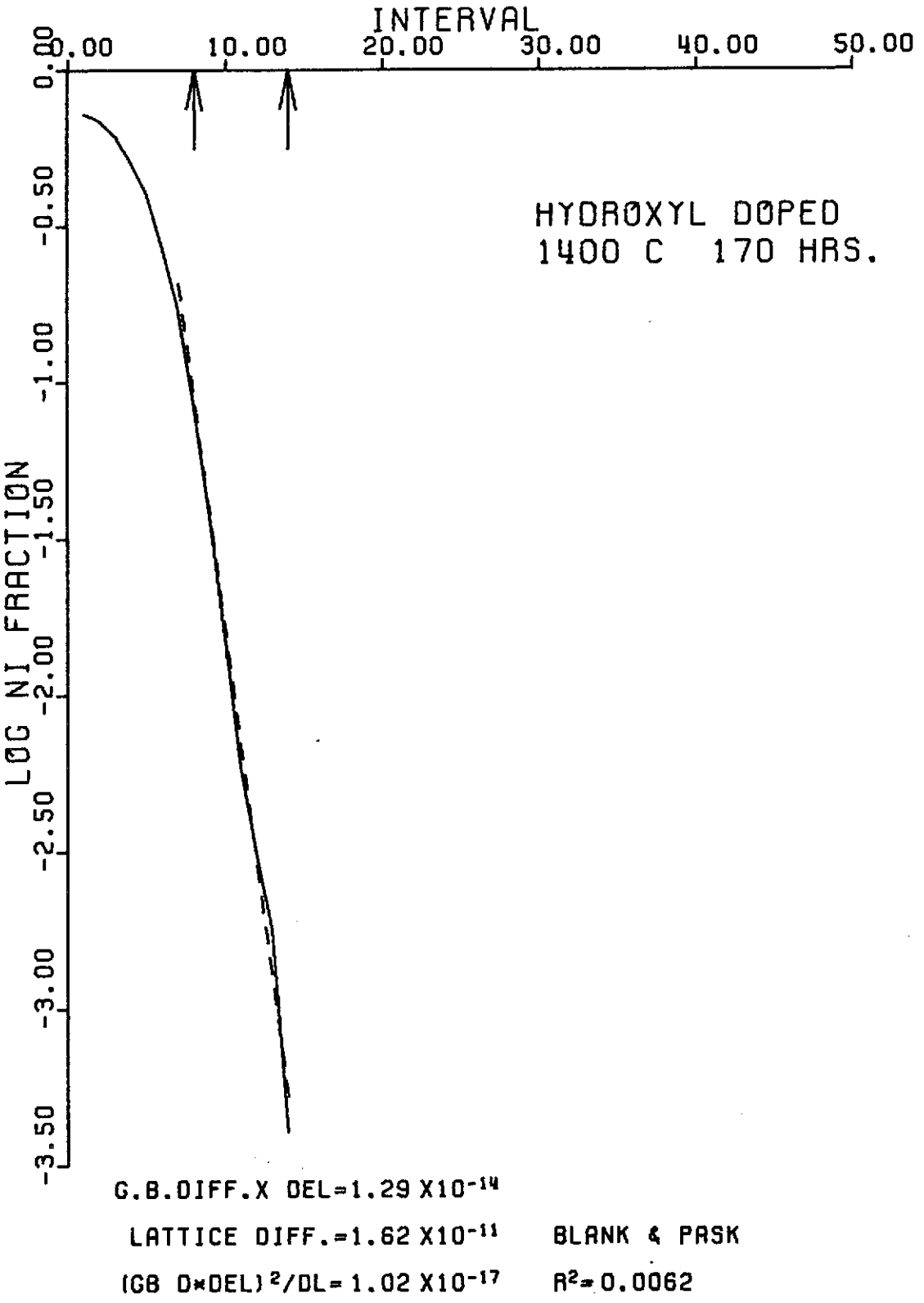

Fig. 1b. Diffusion profile for Ni^{2+} in hydroxyl doped MgO (R^2 is square of standard error)

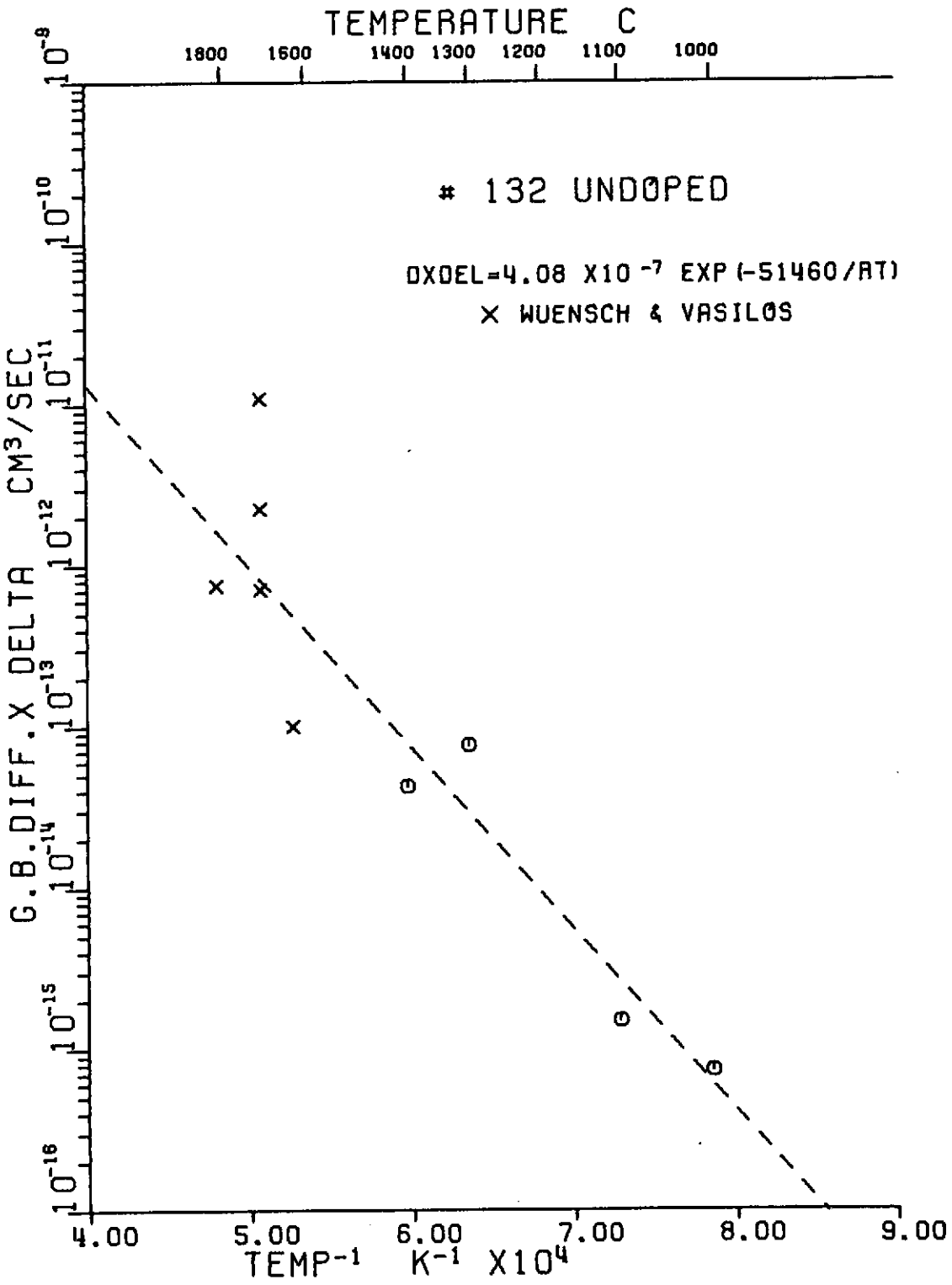

Fig. 2. Diffusion constant versus temperature for Ni^{2+} in undoped MgO

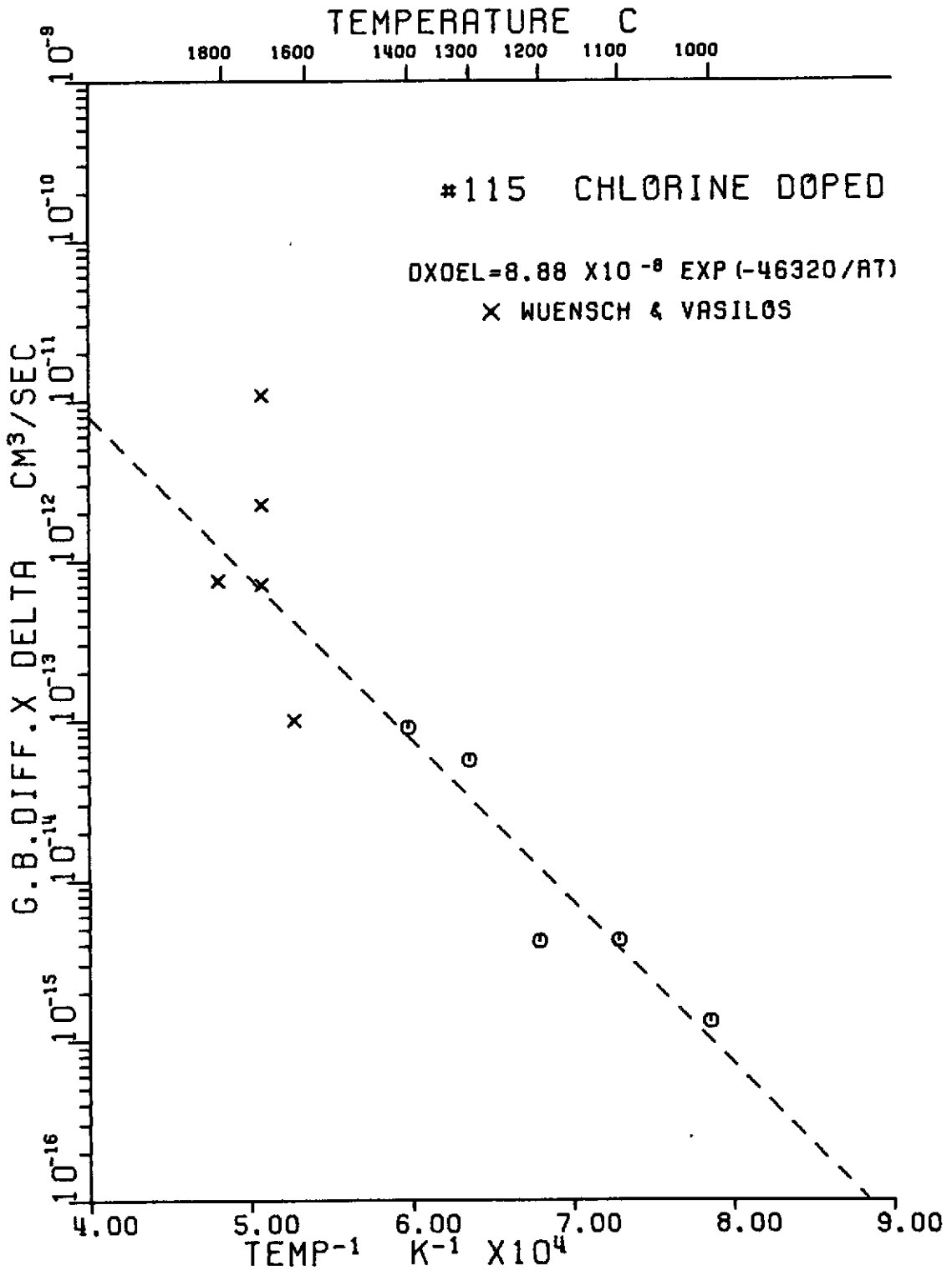

Fig. 3. Diffusion constant versus temperature for Ni^{2+} in chlorine doped MgO

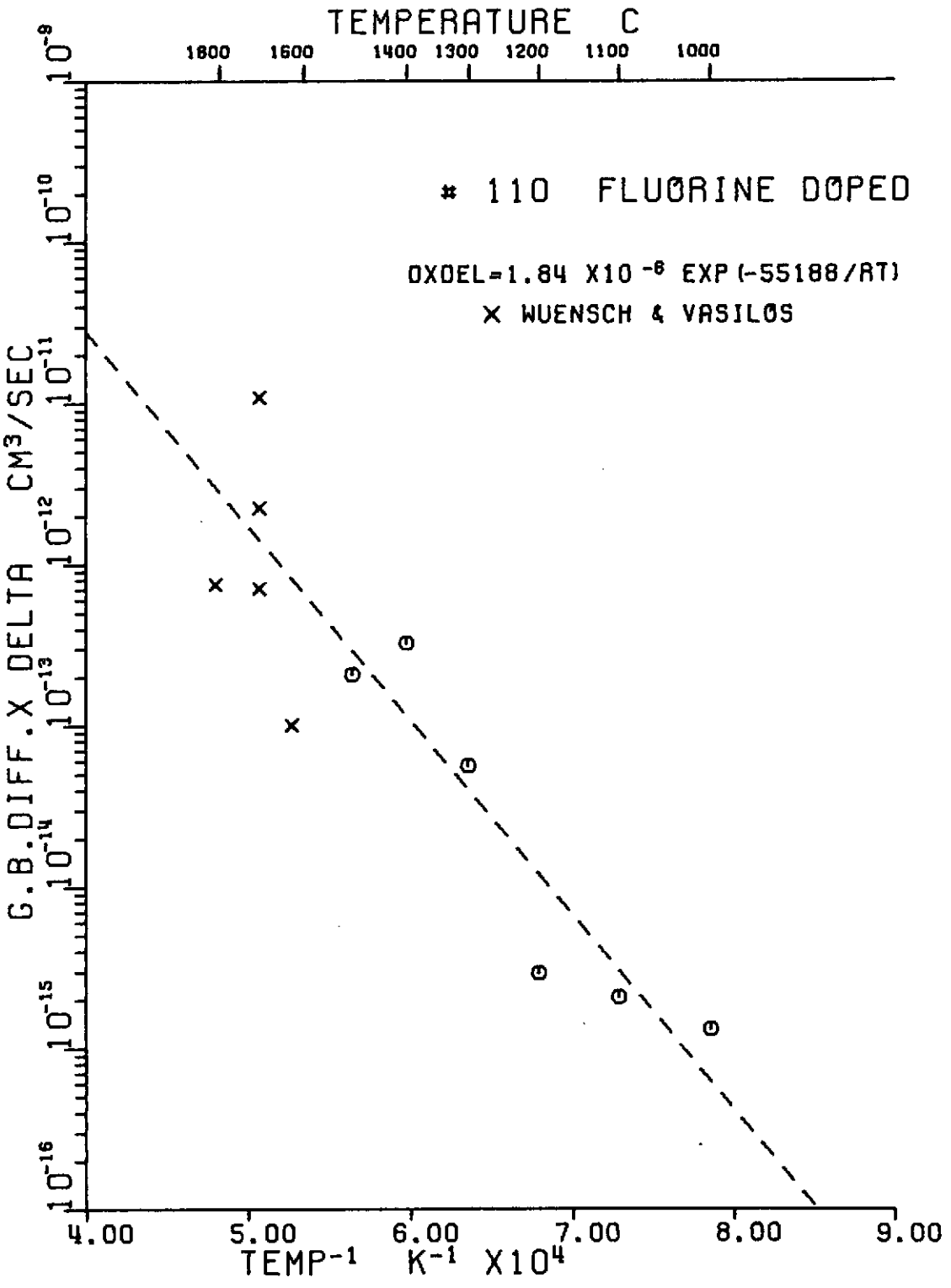

Fig. 4. Diffusion constant versus temperature for Ni^{2+} in fluorine doped MgO

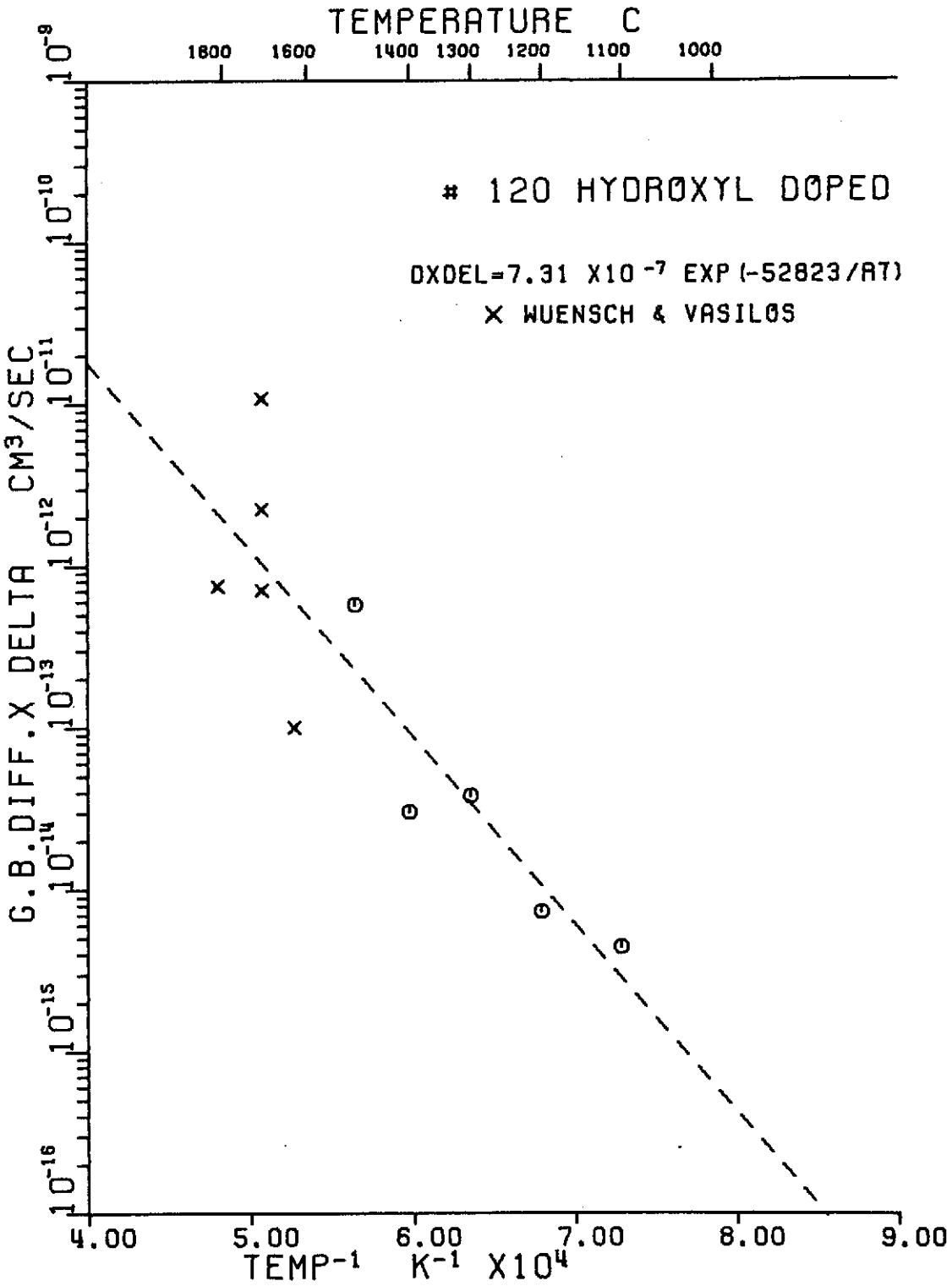

Fig. 5. Diffusion constant versus temperature for Ni^{2+} in hydroxyl doped MgO

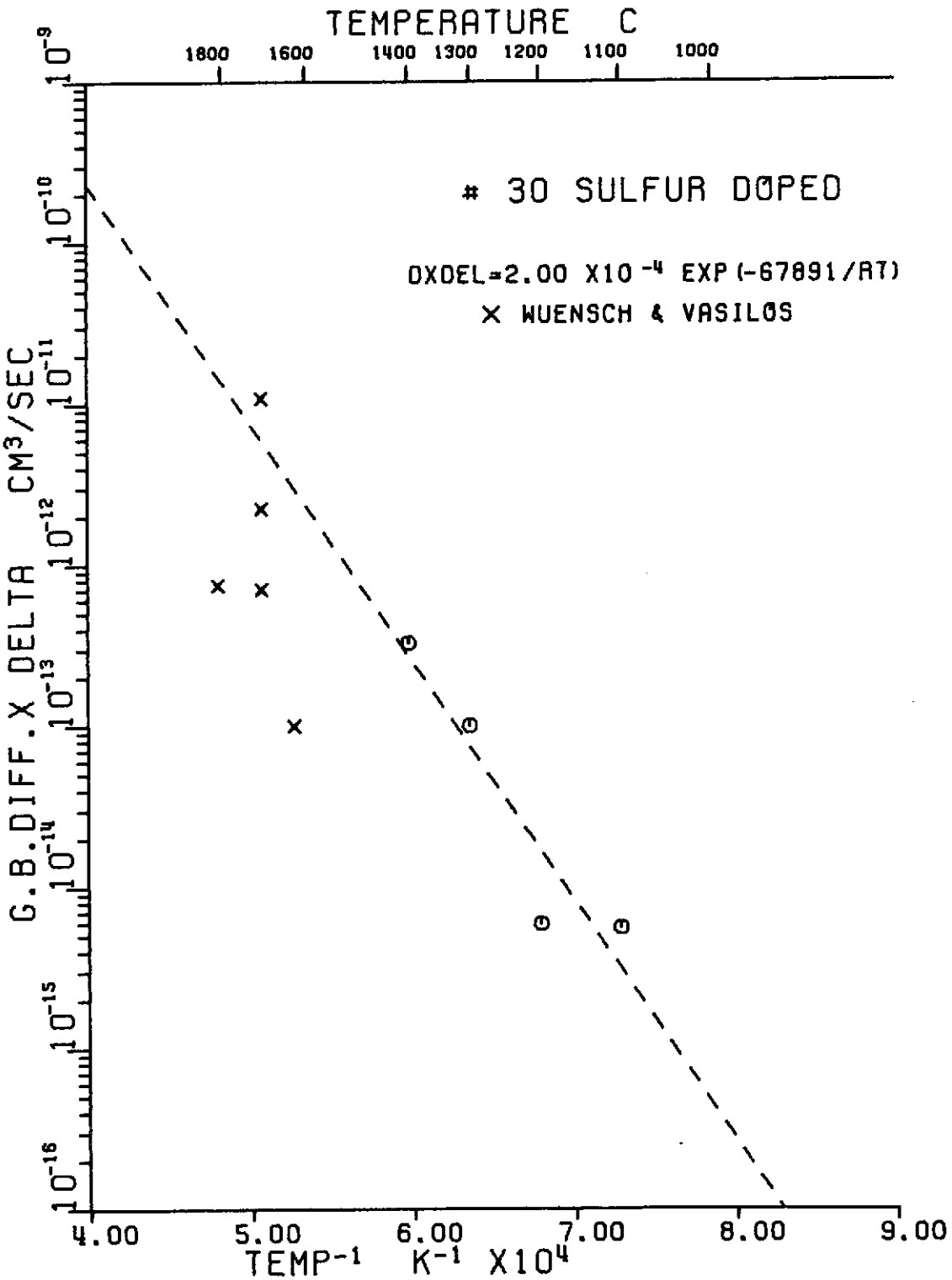

Fig. 6. Diffusion constant versus temperature for Ni^{2+} in sulfur doped MgO

little with various dopants and the undoped control material. There are a number of plausible explanations for this behavior. These are:

1. The anions, while residing at the grain boundaries, do indeed have no effect on the grain boundary diffusion in nickel MgO.
2. The relatively low concentration of anions is uniformly distributed throughout the compact, thus making the concentrations at the grain boundary insignificant.
3. Other impurities in the magnesium oxide determine the grain boundary diffusion behavior, and the contribution of anions is insignificant in comparison.

Attempts were made to define the location of the anions in the compact; results were negative, tending to support No. 2 above. However, negative results are suspect, because sensitivity limits for these anions in the probe are unclear. With respect to Item 1, because of the widely varying physical characteristics of these anions, it is difficult to accept the premise that they all behave essentially identically. From size considerations, fluorine and hydroxyl should be in solution, while chlorine and sulfur should not. Previous results on the role of these anions on densification in MgO agree with the concept, in that chlorine and sulfur were rejected from the lattice into gas phase. It should be emphasized that models based on high energies, binding defects together, could predict a reduction in diffusivity associated with added impurities. However, the results here indicate neither a reduction nor increase.

The information available here, and in the literature, suggest reason No. 2, that the impurity concentration at the boundary is simply too low to introduce

measurable effects. However, the concentration retained was essentially equilibrium, suggesting that with normal processing, anions should not affect grain boundary diffusivity.

III. CARBIDE RESULTS

Silicon nitride and silicon carbide are potentially the best structural materials for high temperature application because of their properties, i. e. high fracture energy, excellent thermal shock resistance, corrosion, and abrasion resistance to a gaseous environment, etc. Slow crack growth is known to occur in some ceramic materials like glass, in which the measured strength depends upon the length of time a load is applied or upon loading rate. Evans and Wiederhorn (Ref. 8), have recently shown that the relationship between the crack velocity and stress intensity factor (K_I) can be used to predict the life-time of a structural component and safe working stress level.

A method of fracture toughness testing, called Constant Moment Beam [CMB], developed by Frieman (Ref. 9), employs a constant moment on the specimen arm even when the crack propagates; this gives a control on crack velocity. In the present study, various grades of silicon carbide and nitride were tested with the CMB method to examine the existence of slow crack growth. The microstructures and fracture surfaces were also examined to correlate the fracture toughness values and the microstructural features.

Previous reports (#10 in Appendix) covered much of the earlier work, and included

1. Design and preparation of a jig for CMB fracture toughness testing.
2. Evaluation of jig performance to determine its mechanical response.
3. Development of a suitable specimen configuration for the application of a constant moment and rigid grip. The formulae for DCB testing (fracture

toughness) and CMB testing (strain energy release rate) were modified for this modified specimen configuration.

4. Testing of glass and plexiglass (PMMA) with DCB and CMB methods with this jig to establish all the experimental details.
5. Development of machining techniques for modified specimen preparation of silicon nitride and carbide for CMB testing.
6. Evaluation and development of suitable etchants after all the etchants available in the literature were tried unsuccessfully.

A. Experimental Procedures

1) Specimen Preparation. Preparation of fracture specimens out of HP Si_3N_4 HS - 130 is extremely time-consuming. To simplify the specimen preparation, easily available materials like glass and plexiglass were used to establish all the experimental details and specimen geometry. These materials were available in sheet form and were easily cut and machined to the desired shape by conventional (plexiglass) or routine diamond (glass) techniques. The glass specimens were with either conventional or modified configuration.

The procedure which was finally developed (Fig. 7) for the preparation of modified specimens of silicon nitride and carbide involved cutting slabs (1-1/2" x 1" x 1") on a precision wafering machine using an available diamond wheel*. Very slow rates were required (.025 depth/pass at 0.125 in/min pass speed) and the wheel required redressing after each pass. A different wheel** was superior (.05 depth/

---

* Norton Co. 5x0.019x0.625D220-M100M-1/8

** Norton Co. 6x0.025x0.625SD160-R100B69-1/8

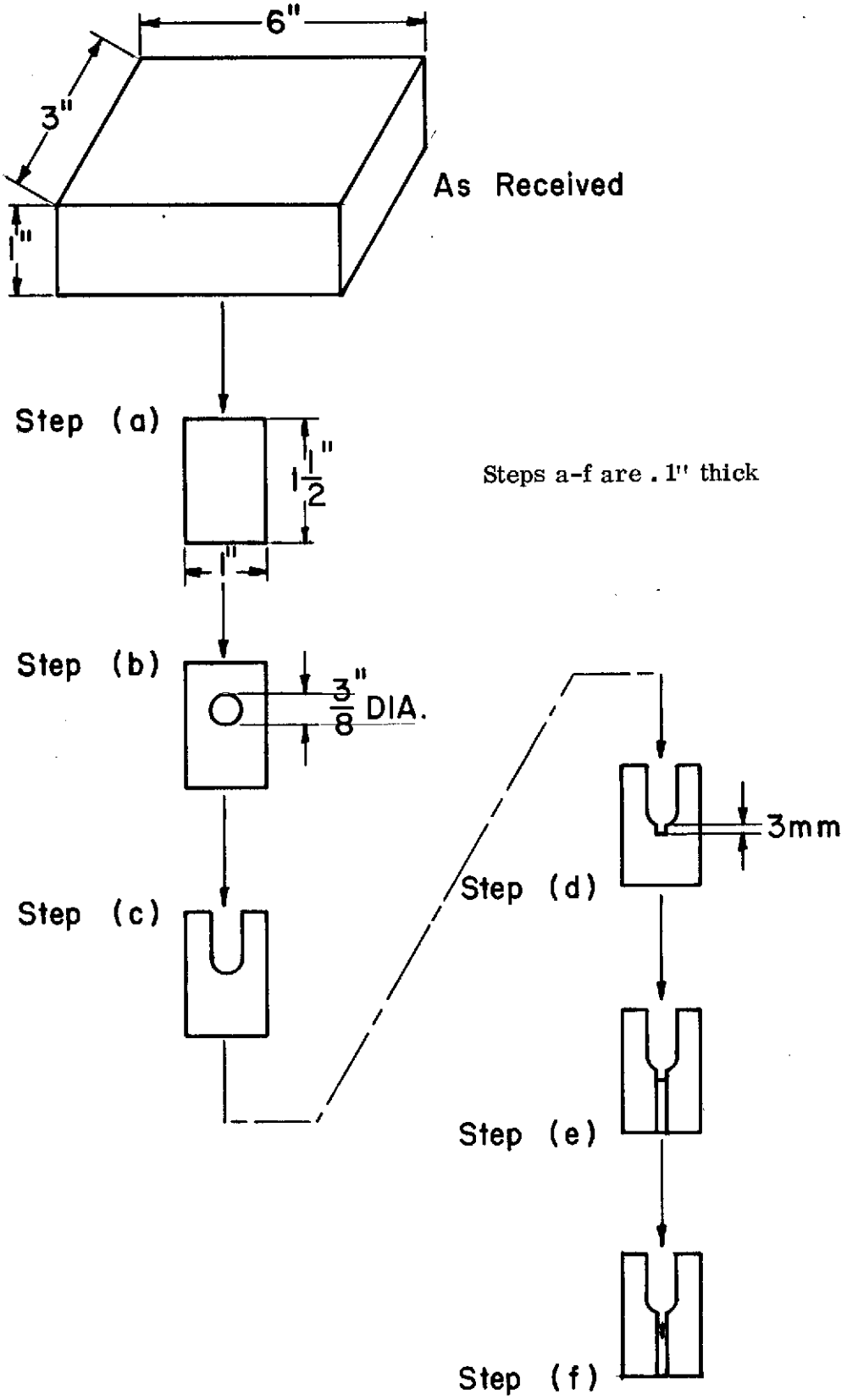

Fig. 7. Machining sequence for modified form of fracture specimen

pass at 0.4 in/min) but redressing was still required.

A diamond core drill (3/8 in. dia.) was used to form the hole (Fig. 7, Step b), and it was necessary to drill part way through from one side, turn the piece over, and finish from the other side to avoid chipping the second surface. A 1/4" core drill was used to smooth the hole interior. The material between the arms was cut with the diamond saw (Fig. 7, Step c).

A groove halfway deep (Fig. 7, Step d) was cut, then a notch was made in the specimen with a diamond drill (Fig. 7, Step e). The length of the notch was found to be critical in ease of producing microcracks. A length of 3-5 mm was found to be ideal.

The last step in making the specimen was to produce a microcrack (Fig. 7, Step f). In either fracture toughness test (CMB or DCB), the specimen was fractured by the extension of a microcrack produced in the specimen. The uncracked specimen was held (lightly tightened) in the middle at a distance of 3 to 4 mm from the tip of the notch with a hardened tool steel clamp, then a load was applied with the tensile testing machine at a crosshead speed of 0.0002 in/min. At a particular load, a crack was produced at the tip of the notch along the side groove and propagated until it was arrested by the compressive stress field produced by the clamp on the specimen. The crack propagation was indicated by a sudden small drop in the load, and exactly at that instant, the crosshead motion was reversed to reduce the load. The distance at which the clamp was tightened from the tip of the notch, the amount of tightening, and the crosshead speed during load application were found to be critical in producing the microcrack. Suitable values were found by trial and error.

After cracking, all specimen dimensions were recorded and the crack length, L, was measured with a microscope.

2) DCB Testing. DCB fracture toughness testing using the modified specimen form was accomplished by using only parts I (the three-line grip) and II of the CMB jig (Fig. 8). The specimen containing the microcrack was held with the grip of part I by tightening the screws. Part II was connected to part I and to the testing machine, thus lying parallel rather than perpendicular to part I. A load was applied to the specimen by downward crosshead motion of the tensile testing machine at a crosshead speed of 0.002 in/min. The load at which the specimen fractured was noted.

3) CMB Testing. The entire CMB assembly (Fig. 8) was used for the constant moment testing. The jig was attached to the Instron and while it was hanging, the

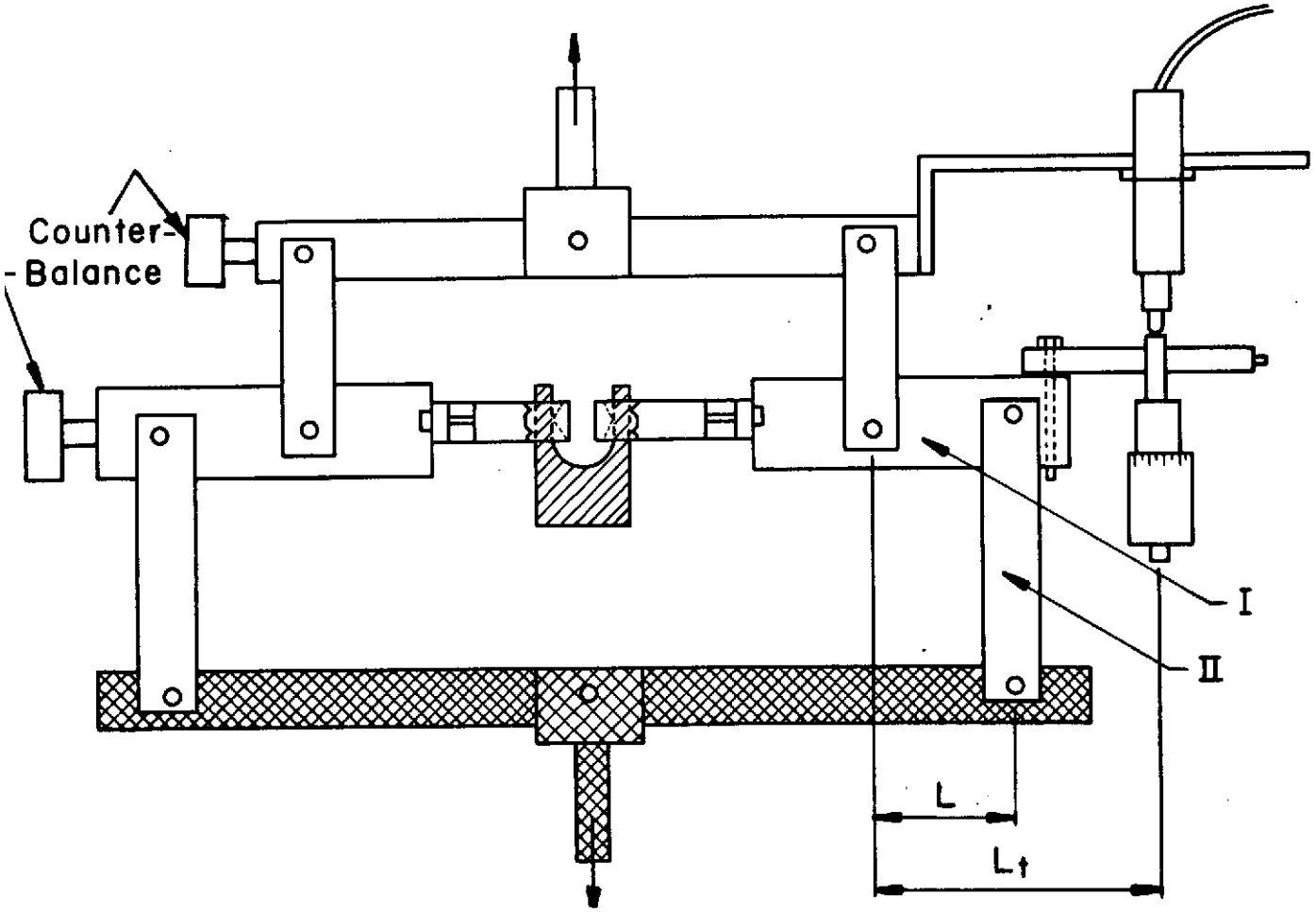

Fig. 8. Schematic drawing of CMB testing jig.

Instron was balanced to zero load, and the transducer used to measure the crack velocity was calibrated. Loading was then started at the desired crosshead speed. The microcrack in the specimen was constantly being observed with a telescope during loading. For glass and plexiglass specimens, it was observed that when the crack started propagating in the specimen, the load almost remained constant until the specimen completely fractured. This constant load (P_1) was used to calculate the toughness value.

The movement of the tip of the transducer during the test was recorded on a chart by feeding the signal from the transducer to obtain a crack velocity. Crosshead speeds of 0.02, 0.002, 0.0002, 0.00002, 0.05, 0.005, and 0.0005 cm/min. were used (the very slow speeds were obtained by special gear reductions to the Instron). In all cases, the fracture surface was carefully preserved.

4) Microstructure Examination. The fracture of a material depends to a great extent on its microstructure. The materials were polished and etched in the following manner to observe the microstructure.

Each specimen mounted on a plastic mold, was polished on successively finer diamond wheels, ranging from 100 mesh to 6 micron. About 2-4 minutes per wheel were used. Then the specimen was polished on a wet cloth with 0.3 micron Alumina powder suspension in water for 15 minutes, and then 0.05 micron Alumina for 10-12 hours in a vibratory polisher.

Several etchants, known in the literature, were tried and an effective etchant was finally obtained. The polished specimen was etched in a boiling mixture of HF, H_2O_2 and HNO_3 (volume ratio of 5:6:1) in a platinum crucible.

The fracture surface of each specimen, produced by the fracture toughness testing, was cut to 2mm x 3mm size by mounting the fractured specimen in wax and using a precision wafering machine. The mounting wax was dissolved in acetone in an ultrasonic cleaner. This fracture surface was observed under SEM.

B. Observations and Results

The observations of DCB fracture toughness testing of conventional and modified glass specimens (Fig. 9 and 10) are listed in Tables III and IV. The values of G_c for both specimen geometries compare very well indicating that the modification of the formula for G_c is correct. Observations of DCB fracture toughness testing of silicon nitride and silicon carbide with modified specimens are presented in Tables V and VI. Observations of CMB fracture toughness testing with modified specimens of glass, plexiglass, silicon nitride and silicon carbide are tabulated in Tables VII to XII.

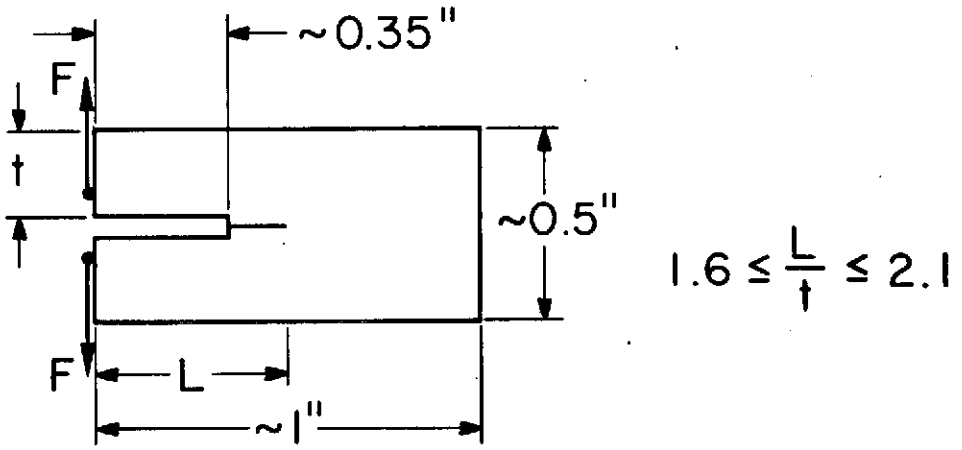

Fig. 9. Conventional specimen configuration

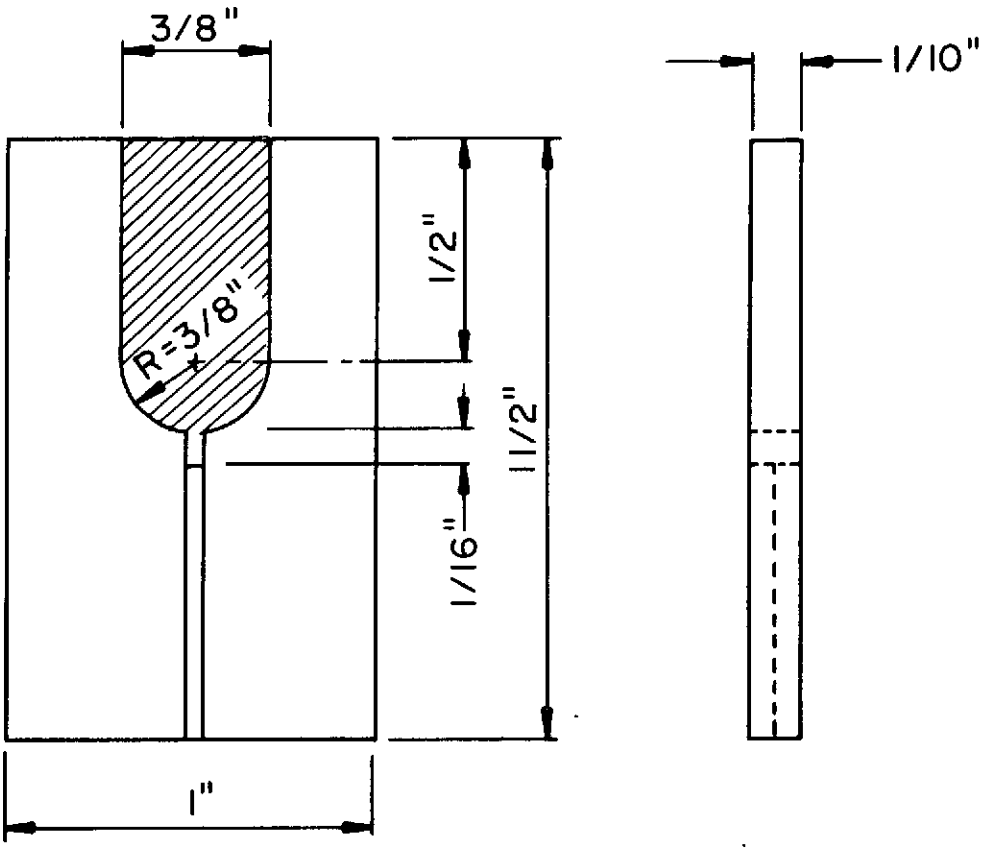

Fig. 10. Modified specimen

Table III. DCB Fracture Toughness Testing of Glass Using Conventional Specimen

Spec. No.	L inch	Mean t inch	b inch	W inch	F lbs.	G_c ergs/cm^2
1	0.41	0.253	0.02	0.0394	1.4	8520
2	0.68	0.238	0.017	0.0394	0.64	8880
3	0.35	0.253	0.022	0.0394	1.34	6860
4	0.39	0.237	0.026	0.0394	1.6	9600

Avg. G_c = 8465 ergs/cm^2

Table IV. Toughness Results for Glass by DCB Technique and Modified Specimen

$E = 81.0 \times 10^{10}$ dynes/cm^2 t = 1.27 cm t* = 0.75 cm

w = 0.3048 cm b = 0.1524 cm

Spec. No.	l cm	L cm	F kg	G_c Conv. ergs/cm^2
1	0.45	2.0	2.6	8947.28
2	0.40	2.05	2.5	9149.4
3	0.43	2.15	2.45	9391.2
4	0.39	2.15	2.40	8502.2
5	0.42	2.10	2.5	9503.3
6	0.39	2.05	2.55	9311.6

Avg. G_c = 9134 ergs/cm^2

Table V. DCB Fracture Toughness Testing, Silicon Nitride

Material: H. P. Si_3N_4 (HS - 130 Norton) $E = 3.12 \times 10^{12}$ dynes/cm^2

Method of testing: DCB t = 1.27 cm

Specimen configuration: Modified t* = 0.75 cm

Spec. No.	W cm	l cm	b cm	L cm	F kg	G_c Conv. ergs/cm^2
1	0.294	0.775	0.155	1.324	15.0	75744.0
2	0.2415	0.975	0.127	1.360	12.7	90793.8
3	0.297	0.825	0.163	1.274	21.9	84432.1

Avg. G_c = 83656.6 ergs/cm^2

Table VI. DCB Fracture Toughness Testing, Silicon Carbide

Material: SiC (Refel)

Test: DCB

Specimen configuration: Modified

Density = 3.06 gm/cm^3 E = 3.66 x 10^{12} dynes/cm^2

t = 1.15 cm t* = 0.7 cm

Spec. No.	W in	b in	l cm	L cm	F kg	G_c Conv. ergs/cm^2
1	0.12	0.06	0.74	1.26	16.2	76151.9
2	0.115	0.057	0.82	1.31	15.6	80384.2
3	0.12	0.062	0.76	1.29	16.6	81228.5

Avg. G_c = 79254.9 ergs/cm^2

Table VII. Toughness Results for Glass by CMB Technique and Modified Specimen

Spec. No.	Crosshead speed in/min.	P_1 kg	$\frac{d\delta}{dT}$ est. in/min. x 10^4	$\frac{d\delta}{dT}$ experimental in/min.	G mod ergs/cm^2	Crack vel in/min.
1	0.0005	2.2		13.3×10^{-4}	7362.7	0.01848
2	0.0005	2.1	~0.39	13.05×10^{-4}	6961.6	0.01865
3	0.0005	2.15		13.21×10^{-4}	7160.6	0.01862
4	0.005	2.35	~ 3.7	15.1×10^{-3}	7986.0	0.2015
5	0.005	2.35		14.95×10^{-3}	7986.0	0.19955
6	0.005	2.3		14.5×10^{-3}	7775.4	0.19615
7	0.05	2.6	~ 36.0	28.6×10^{-2}	9082.0	3.5798
8	0.05	2.5		27.2×10^{-2}	8636.0	3.4914
9	0.05	2.55		29.1×10^{-2}	8857.0	3.68828
10	0.05	Broke on side				
11	0.0002 cm/min	2.05	0.16	5.1×10^{-4}	6742.4	0.002783
12	0.00002 cm/min	1.9	0.02	6.2×10^{-5}	6221.64	0.00034

$\frac{d\delta}{dT}$ est. obtained from page 46

Table VIII. Toughness Results for Plexiglass (PMMA) by CMB Technique Using Modified Specimen

$E = 2.77 \times 10^{10}$ dynes/cm^2

W = 0.11 in b = 0.055 in t = 1.27 cm t* = 0.75 cm

l = 0.4 cm L_c = 3.81 cm L_m = 7.7 cm

Spec. No.	Crosshead Speed cm/min.	P_1 kg	$\frac{d\delta}{dT}$ est. in/min.	$\frac{d\delta}{dT}$ experimental in/min.	Crack vel mm/sec	G mod ergs/cm^2	K_I $\frac{10^7 \text{ dyne}}{\text{cm}^{3/2}}$
1	0.2	3.4				475,112	11.4
2	0.2	3.5				491,974	11.65
3	0.2	3.5	~0.12			491,974	11.65
4	0.2	3.35				468,421	11.35
5	0.2	3.6				512,281	11.9
6	0.02	3.2	~0.0168	0.082	0.238	427,421	10.85
7	0.02	3.25		0.088	0.231	446,049	11.1
8	0.02	3.2		0.081	0.220	427,421	10.84
9	0.02	3.15		0.0804	0.209	406,493	10.58
10	0.02	3.2		0.0813	0.225	406,049	10.58

Table VIII (continued)

Spec. No.	Crosshead Speed cm/min.	P_1 kg	$\frac{d\delta}{dT}$ est. in/min.	$\frac{d\delta}{dT}$ experimental in/min.	Crack vel mm/sec	G mod ergs/cm^2	K_I $\frac{10^7 \text{ dyne}}{\text{cm}^{3/2}}$
11	0.005	2.8	~0.00361	0.0196	0.0252	364,161	10.0
12	0.005	2.7		0.0226	0.0242	347,120	9.78
13	0.005	2.7		0.020	0.0232	347,120	9.78
14	0.005	2.9		0.0185	0.0231	381,661	10.25
15	0.005	2.85		0.0201	0.0283	372,872	10.12
16	0.002	2.6	~0.0017	0.0087	0.00510	330,464	9.55
17	0.002	2.55		0.0085	0.00633	322,290	9.41
18	0.002	2.6		0.0096	0.00558	330,464	9.55
19	0.002	2.4		0.0077	0.00596	314,217	9.3
20	0.002	2.5		0.0082	0.00672	298,380	7.57
21	0.0002	2.3	~0.00014	0.00065	0.00016	282,952	8.82
22	0.00002	2.1	~0.00001	0.000073	0.000023	253,326	8.35

Table IX. Toughness Results by CMB Technique for Si_3N_4

Material: H. P. Si_3N_4 (HS - 130 Norton)

Test: CMB

Specimen configuration: Modified

$E = 3.12 \times 10^{12}$ dynes/cm^2

$t = 1.27$ cm $\qquad$ $t^* = 0.75$ cm

$l = 1.0$ cm $\qquad$ $L_c = 3.81$ cm

Spec. No.	W cm	b cm	Crosshead Speed cm/min	P_1 kg	G_c Mod ergs/cm^2
1	0.259	0.132	0.02	16.1	74358.6
2	0.104	0.104	0.002	14.1	83347.1
3	0.252	0.125	0.0002	14.8	69192.2
4	0.263	0.132	0.00002	15.13	66716.2
5	0.260	0.135	0.005	17.7	86119.3
6	0.262	0.131	0.0005	16.1	74251.3
7	0.242	0.120	0.0002	16.1	87431.3
8	0.164	0.082	0.00002	9.7	76046.2
9	0.281	0.145	0.0005	17.8	74996.7

Avg. $G_c = 76976$

Table X. Toughness Results by CMB Technique for SiC

Material: SiC (Refel) l = 1.5 cm

Test: CMB t* = 0.7 cm

t = 1.15 cm L_c = 3.81 cm

Spec. No.	W in	b in	Crosshead Speed cm/min.	P_1 kg	G Mod ergs/cm^2
1	0.11	0.055	0.00002	15.2	81113.3
2	0.12	0.006	0.0002	16.3	77365.8
3	0.084	0.042	0.0002	11.5	82875.4
4	0.105	0.053	0.009	14.4	79491.5
5	0.12	0.062	0.00002	17.0	83518.0

Avg. G_c = 79228

Table XI. Toughness Results by CMB Technique for SiC

Material: SiC (Ceradyne) Density = 3.04 g/cm^3 t* = 0.7 cm

Method: CMB E = 3.64 x 10^{12} dynes/cm^2 t = 1.15 cm

Specimen configuration: Modified l = 1.5 cm L_c = 3.81 cm

Spec. No.	W in	b in	Crosshead Speed cm/min.	P_1 kg	G Mod ergs/cm^2
1	0.154	0.077	0.002	21.0	75237.6
2	0.154	0.077	0.0002	21.8	80202.9
3	0.154	0.077	0.00002	21.9	80764.4

Avg. G_c = 78734

Table XII. Toughness Results by CMB Technique, Summary

Test: CMB

Specimen configuration: Modified

$t = 1.27$ cm $\qquad t^* = 0.75$ cm

$l = 1.0$ cm $\qquad L_c = 3.81$ cm

Material	Density g/cc	E 10^{12} dynes/cm^2	W in	b in	Crosshead Speed in/min.	P_1 kg	G_c ergs/cm^2
Silicon Carbide							
Carborundum	2.98	3.54	0.105	0.053	0.0002	12.4	60541
Norton							
A	3.10	3.70	0.086	0.043	0.0002	11.9	86441
B	3.10	3.70	0.09	0.045	0.00005	12.2	90303
Silicon Nitride							
AVCO	3.10	3.12	0.260 cm	0.131 cm	0.00005	16.0	74196

Slow crack growth was observed for both glass and plexiglass. The crack velocity was determined by obtaining the rate of change of deflection, $\frac{d\delta}{dT}$, of the tip of the transducer. During the application of load, there was a very small rate of change of deflection until the crack started to propagate. As the crack propagated, the load remained almost constant and $\frac{d\delta}{dT}$ remained constant, but had a value much higher than that before crack propagation. This $\frac{d\delta}{dT}$ was used to calculate the crack velocity and the constant load P_1 to calculate the strain energy release rate.

As the crack approached the end of the specimen, the fracture became catastrophic, the load suddenly dropped to zero, and $\frac{d\delta}{dT}$, corresponding to this period, could not be measured.

The values of strain energy release rate G are plotted vs. crack velocities for glass in Fig. 11. The plot shows that with increased crosshead speed or loading rate, both the crack velocity and strain energy release rate increased.

In all silicon nitride and carbide tests, it was observed that the load increased continuously, the rate of increase depending on the crosshead speed. The load did not remain constant during any period, and it dropped suddenly to zero at the time of fracture of the specimen, which was catastrophic. No slow crack growth was observed with the telescopic observations. The values of fracture toughness obtained do not show any definite dependence on crosshead speed or loading rate (Tables IX-XI). They are in agreement with the values obtained by DCB fracture toughness testing.

C. Discussion of the Results

1) Behavior of Glass. The values of strain energy release rate plotted vs. crack velocity in case of glass, are compared with those in the literature.

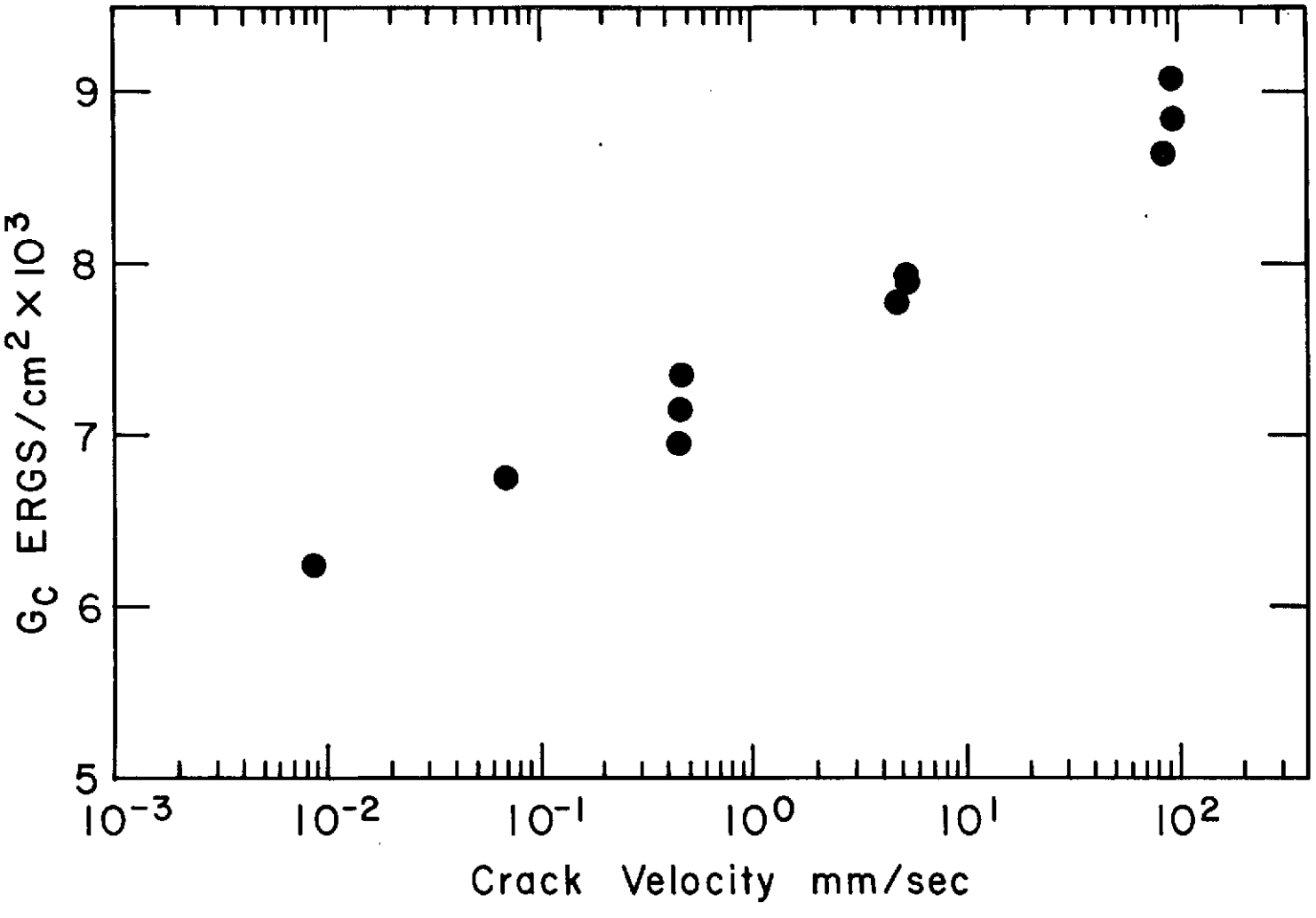

Fig. 11. G_c for slow crack growth in glass microscope slides in room air using constant moment test

The exponential dependence of strain energy release rate G on crack velocity in the case of glass, can be explained on the basis of Charles and Hillig theory for slow crack growth in glass (Ref. 10). According to their theory, the crack velocity is given by

$$V = V_o \exp - \left[E^*(o) + \Gamma V_m/\rho - \sigma V^* \right] / RT$$

where $E^*(o)$ is the activation energy for surface dissolution at a stress free surface.

$\Gamma V_m/\rho$ represents the effect of the surface tension in retarding crack motion, where σ is the surface free energy of the glass corrosion product interface, V_m is the molar volume of glass and ρ is the radius of curvature of the crack tip.

$V^* = \left(\frac{\partial E^*}{\partial \sigma}\right)\sigma = 0$ has the units of volume and is considered as activation volume. T is the temperature, R is the gas constant, V_o is a constant, and σ is the stress acting at the crack tip. Therefore, the functional dependence of crack velocity on the σ can be expressed as

$$C = A \exp - \left[B - \sigma \right]$$

where A and B are constants.

$$\text{That is, } V = A \exp \left[\sigma - B \right]$$

Now the stress intensity factor K_1 is directly dependent on the stress at the crack tip and is related to strain energy release rate G by $K_1^2 = 2 EG_1$, as previously mentioned. So the exponental increase of G with crack velocity is expected (Fig. 11).

The nature of the plot of G vs. crack velocity obtained by Frieman also has the same nature. The difference in G values (Fig. 11) corresponding to a particular crack velocity is probably due to the different humidity conditions at which the testing was done.

2) Behavior of Plexiglass. In the case of plexiglass, the elastic modulus is time dependent (Ref. 11) and so the stress intensity factor K_1 was calculated back from values of G vs. crack velocity, and was plotted in Fig. 12. Marshall and Williams have shown that crack speed can have a considerable effect on toughness because of the sensitivity of modulus E and yield stress σ_y of plexiglass to changes

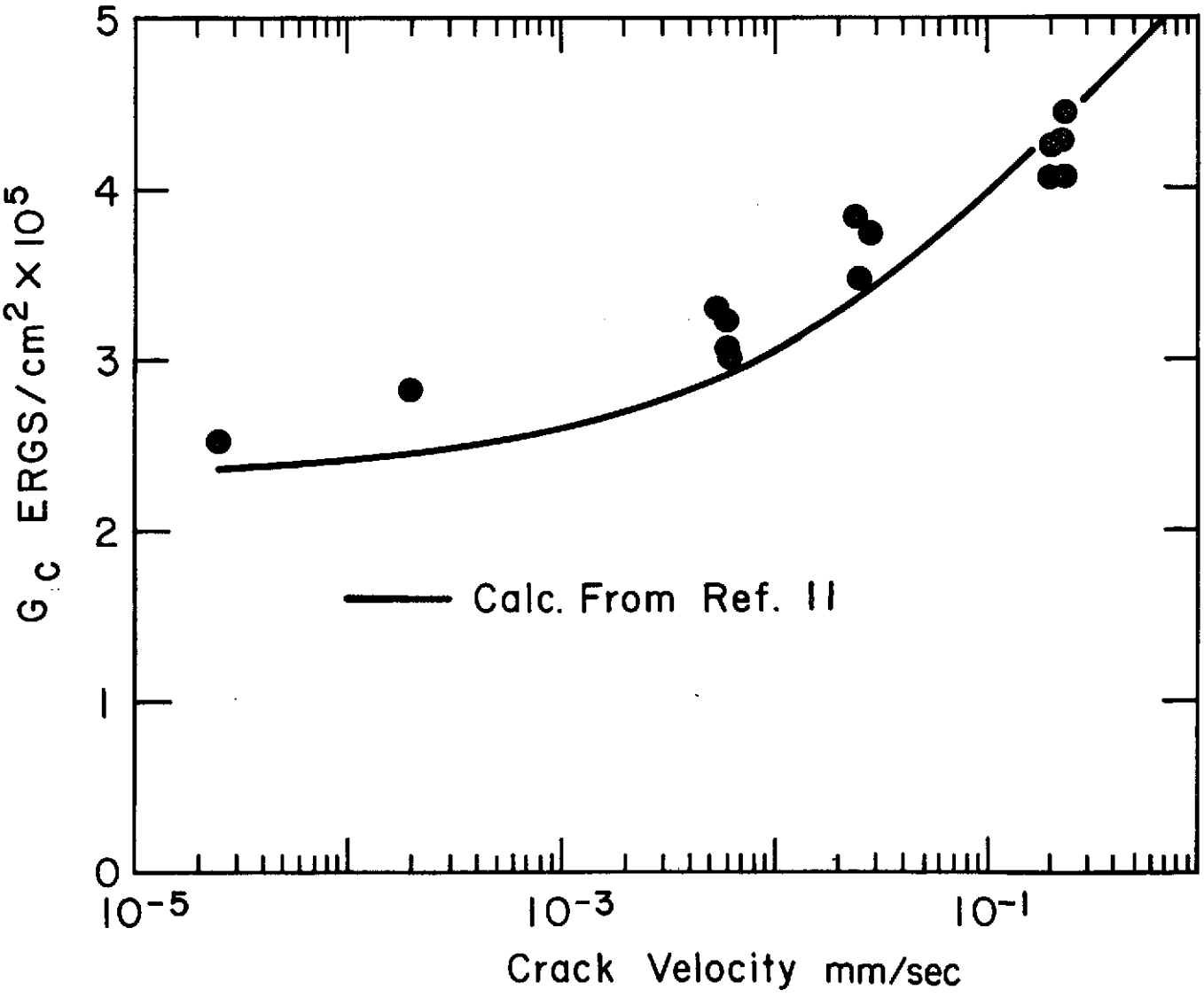

Fig. 12. G_c for slow crack growth in plexiglass in room air using constant moment test

in straining rate. As a crack accelerates there is a corresponding increase in the straining rate at the crack tip, resulting in an increase in E and σy, thereby producing an increase in K_{ic}. The present results agree with those published in the literature (Fig. 12).

The agreement of results on glass and plexiglass with the published results indicate that the CMB fracture toughness testing using modified specimen, the jig, and the specimen geometry designed for the application of this technique are suitable for studying the slow crack growth in a material.

3) Behavior of Silicon Nitride and Silicon Carbide. As mentioned earlier, tests on silicon nitride and carbide did not show evidence of slow crack growth. However, the steady increase in the load indicated by the Instron, had produced a constant rate of deflection $\frac{d\delta}{dT}$ of the tip of the transducer. The source of this deflection was analyzed in the following manner, in order to determine if any observed deflection was due to crack propagation.

Prior to fracture, in the absence of slow crack growth, the deflection δ_{el} indicated by the transducer consisted of two parts:

$$\delta_{el} = \delta_s + \delta_j$$

where δ_s is due to the elastic deflection of the specimen due to the applied bending moment and δ_j is due to the elastic deformation of the jig itself;

$$\therefore \frac{d\delta}{dT} = \frac{d\delta_s}{dT} + \frac{d\delta_j}{dT}$$

During the evaluation of the performance of the jig, δ_j vs. load curve was plotted (Fig. 13). The slope of this curve gives $\frac{d\delta_j}{dF}$. From the load time curve,

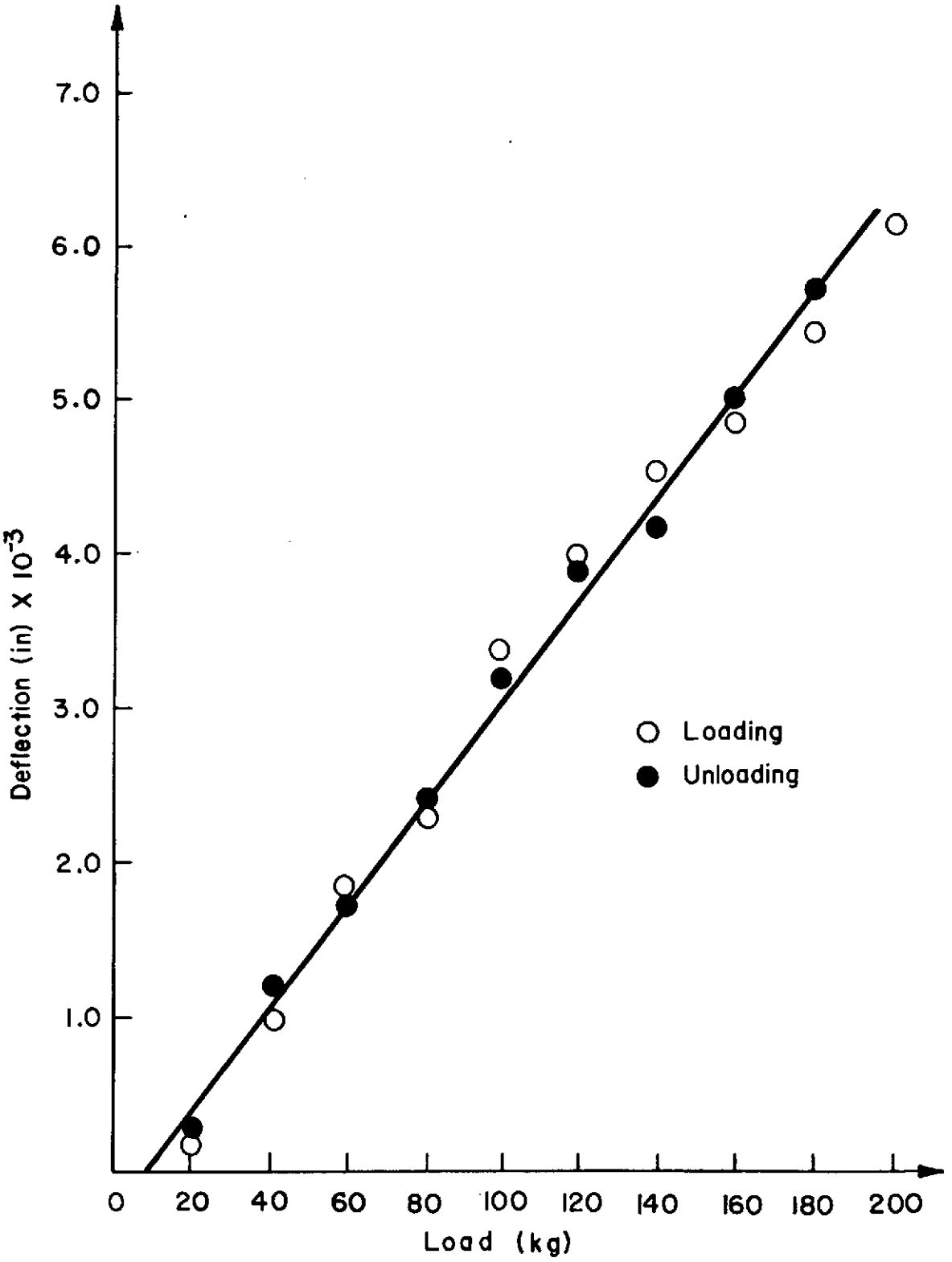

Fig. 13. Indicated deflection of CMB jig versus load. Elastic deflection of specimen eliminated by plates bolted to opposite sides of part I in Fig. 8.

$\frac{dF}{dT}$ is obtained and

$$\frac{d\delta_j}{dT} = \frac{d\delta_j}{dF} \cdot \frac{dF}{dT}$$

So $\frac{d\delta_j}{dT}$ can be obtained.

Also, the rate of change of moment $\frac{dM}{dT}$ applied on the specimen arm can be obtained, and, using the elastic theory of bending of beams, an estimate of $\frac{d\delta_s}{dT}$ is obtained.

Relationship between rate of change of deflection and rate of change of moment (Fig. 14):

If b = elastic deflection of the specimen

δ_s = deflection of the transducer due to elastic deformation of specimen arm

L_t = distance of the transducer from the fulcrum

$$\theta_1 = \theta_2 \simeq \tan \theta_2 = \frac{b}{a} = -\frac{\delta}{L_t}$$

$$\theta = -\frac{Mx}{EI}$$

For $x = a$, $\theta_1 = -\frac{Ma}{EI}$

$$\therefore b = \frac{Ma^2}{EI}$$

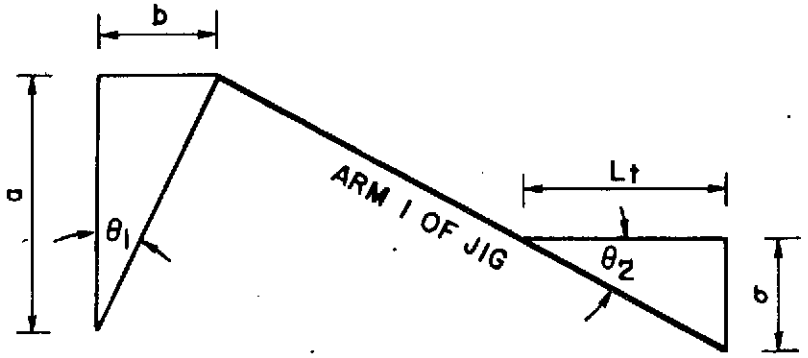

Fig. 14. Schematic relationship between elastic deflection of specimen and deflection indicated by transducer

Also

$$\delta_s = \frac{a\, L_t}{EI} M$$

$$\therefore \frac{d\delta_s}{dT} = \frac{a\, L_t}{EI} \frac{dM}{dT}$$

since a, L_t, and I are constant prior to crack propagation. For this configuration, we can then calculate

$$\therefore \frac{d\delta}{dT} = \frac{d\delta_{el}}{dt} = \frac{d\delta_s}{dt} + \frac{d\delta_j}{dt} = \frac{aL_t}{EI} \frac{dM}{dT} + \frac{d\delta_j}{dF} \times \frac{dF}{dT}$$

and using measured values of $\frac{dM}{dT}$ for each data set, $\frac{d\delta_j}{dF}$ from initial jig evaluation (Fig. 14) and A, L_t, E, and I from the specimen, it was determined that calculated elastic deflections and observed deflections agreed within a scatter of ±10%. These are summarized in Table XIII. This was one confirmation of lack of slow crack growth.

To further evaluate the question of slow crack growth occurring in these materials, the specimen was subjected to a constant load over a long period of time.

Specifically, a modified specimen of SiC (Refel) with dimensions t = 1.15 cm, t* = 0.7 cm, w = 0.067 in., b = 0.033 in. was subjected to load 10.4 kg = P_1 using the modified method (CMB) with l = 1.5 cm, L_c = 3.81 cm. This load corresponds to 80% of G_c average (80,000 ergs/cm^2) for SiC (Refel). Initially, the load was applied with a crosshead speed of 0.0002 cm/min. When the load reached 10.5 kg, the crosshead motion was stopped and the specimen was left loaded for one day. No decrease in load was observed during this time except in the first 2-3 minutes in which the load dropped to 10.4 kg due to the testing machine. When loading was started again, maintaining a crosshead speed of 0.0002 cm/min., the specimen

Table XIII. Calculated Elastic Deformation During Test $\left(\frac{d\delta}{dT}\right)$ and Observed Deformation $\left(\frac{d\delta_{ob}}{dT}\right)$

Material: H. P. Si_3N_4 (HS - 130 Norton) Specimen: Modified

Test: CMB $\frac{d\delta_j}{dF} = 3 \times 10^{-5}$ in/kg

Spec. No.	Crosshead Speed cm/min.	$\frac{dM}{dT}$ kg-cm min.	$\frac{d\delta_j}{dT}$ in/min. x 10^5	$\frac{d\delta_s}{dT}$ in/min. x 10^5	$\frac{d\delta}{dT}$ est. in/min. x 10^5	$\frac{d\delta_{ob}}{dT}$ experimental in/min. x 10^5
1	0.02	24.8	19.5	33.7	53.2	50.3
2	0.002	2.51	1.97	3.81	5.78	5.45
3	0.0002	0.251	0.197	0.349	0.546	0.502
4	0.00002	0.024	0.018	0.032	0.05	0.046
5	0.005	6.24	4.91	8.41	13.3	12.46
6	0.0005	0.629	0.495	0.841	1.33	1.20
7	0.0002	0.251	0.197	0.359	0.556	0.527
8	0.00002	0.024	0.018	0.052	0.07	0.066
9	0.0005	0.629	0.495	0.783	1.27	1.01
Material: SiC (ceradyne)						
1	0.002	2.54	2.0	2.62	4.62	4.23
2	0.0002	0.255	0.2	0.259	0.459	0.43
3	0.00002	0.0259	0.02	0.026	0.046	0.0415
Material: SiC (Refel)						
1	0.00002	0.025	0.019	0.036	0.055	0.049
2	0.0002	0.256	0.201	0.338	0.539	0.51
3	0.0002	0.259	0.203	0.487	0.60	0.656
4	0.002	2.61	2.05	3.93	5.98	5.21
5	0.00002	0.025	0.052	0.019	0.033	0.047

fractured suddenly at P_1 = 11.2 kg, giving a value of fracture toughness G_c as 76190 ergs/cm^2. That is, the specimen was loaded for one day at a load corresponding to 87.6% of the observed value of G_c. If slow crack growth had taken place in the specimen, the load would have slowly dropped as the crack proceeded. Since this did not occur, lack of slow crack growth is again indicated.

The scatter in the observed values of fracture toughness for silicon nitride and carbide must be due to the inhomogeneities in the material. In homogeneous materials like glass and plexiglass, the scatter was much less.

4) Microstructure and Fracture Surface Examination. The polished and etched microstructures of various silicon carbide and silicon nitride materials are shown in Figs. 15-18. Average grain size and grain morphology (equiaxed or elongated) of these materials are shown in Table XIV. Etched surfaces of Refel SiC and AVCO Si_3N_4 did not produce good microstructures. Any other etchants could not be tried due to lack of knowledge of effective etchants. All silicon carbides show the presence of a second phase which may correspond to the additives used during the densification of these materials.

The fracture surface of the materials produced during the fracture toughness testing are shown in Figs. 19-25. The mode of fracture (transgranular or intergranular) and surface topography are shown in Table XIV. Cleavage steps and river patterns are visible in case of transgranular fracture. The surface is rougher when the fracture mode is intergranular, rather than transgranular.

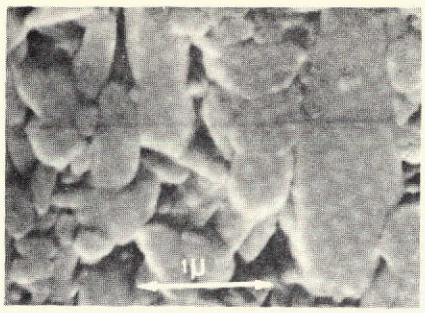

FIG. 15
POLISHED AND ETCHED MICROSTRUCTURE
OF NORTON HS-130 SILICON NITRIDE
(10,500X)

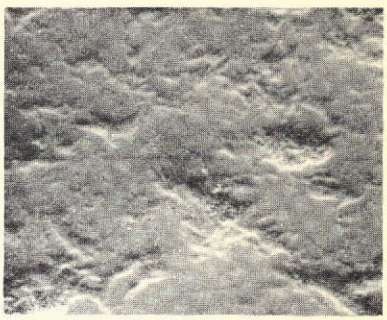

FIG. 16
POLISHED AND ETCHED MICROSTRUCTURE
OF AVCO SILICON NITRIDE (1000 X)

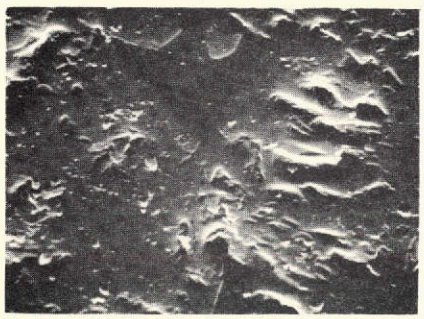

FIG. 17
POLISHED AND ETCHED MICROSTRUCTURE
OF REFEL SILICON CARBIDE (1010 X)

FIG. 18
POLISHED AND ETCHED MICROSTRUCTURE
OF CARBORUNDUM SILICON CARBIDE (112 X)

FIG. 19
POLISHED AND ETCHED MICROSTRUCTURE
OF NORTON SILICON CARBIDE (5700 X)

FIG. 20
FRACTURE SURFACE OF CERADYNE
SILICON CARBIDE (1150X)

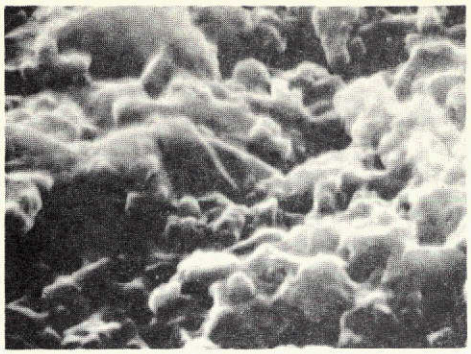

FIG. 21

FRACTURE SURFACE OF NORTON HS-130 SILICON NITRIDE (22000 X)

FIG. 22

FRACTURE SURFACE OF AVCO SILICON NITRIDE (5600 X)

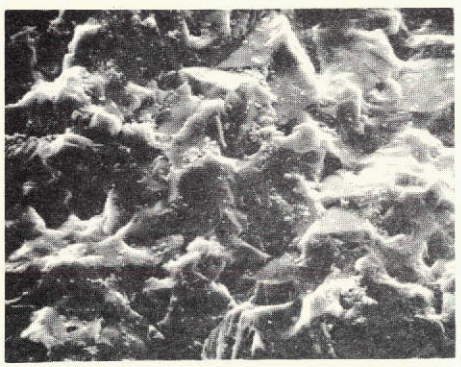

FIG. 23

FRACTURE SURFACE OF REFEL SILICON CARBIDE (1190 X)

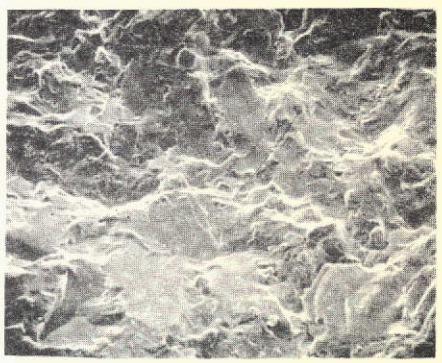

FIG. 24

FRACTURE SURFACE OF CARBORUNDUM SILICON CARBIDE (205 X)

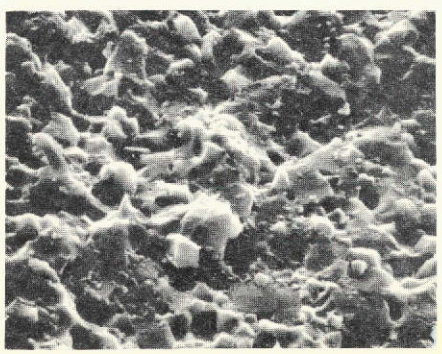

FIG. 25

FRACTURE SURFACE OF NORTON SILICON CARBIDE (2260 X)

Table XIV. Average Grain Size and Grain Morphology

Material	Density g/cc	Grain Size Microns	Grain Morphology	Mode of Fracture	Fracture Topography	Fracture Toughness ergs/cm^2
Silicon Carbide						
A. Carborundum	2.98	50	Equiaxed	Transgranular.	Smooth	60541
B. Norton	3.1	2	Equiaxed	Intergranular.	Rough	88372
C. Ceradyne	3.04	10	Elongated and equiaxed	Intergranular.	Rough	78734
D. Refel	3.06	10	Equiaxed	Partly Intergranular and Partly Transgranular.	Rough	79288
Silicon Nitride						
A. HS-130 Norton	3.12	1	Elongated and equiaxed.	Intergranular.	Rough	76976
B. AVCO	3.10	5	Equiaxed	Intergranular	Rough	74196

D. Correlation between Fracture Toughness Values, Microstructure, and Fracture Surface.

The average fracture toughness values of the silicon carbide and silicon nitride materials are shown along with the density, grain size, grain morphology, mode of fracture and fracture topography in Table XIV. Microstructures are given in Figs. 15-25.

Ceradyne and Refel silicon carbides have almost equal fracture toughness values, 78734 and 79288 ergs/cm^2, respectively, and grain sizes,10 microns, are also equal. Both of them show rough fracture surfaces. Even though Ceradyne contains some elongated grains and shows entirely intergranular fracture, it does not seem to produce a rougher fracture surface which would absorb higher energy during fracture.

Norton silicon carbide has a higher density (3.1 g/cc), and smaller grain size, 2 microns. The fracture is completely intergranular and produces a rough surface. Even though it is difficult to determine from the fracture surface photographs, It can be easily seen that complete intergranular fracture of a material with smaller grain size will produce a larger amount of fracture surface area than that with a courser grain size. For this reason it will absorb higher amounts of energy per unit of apparent area and will have a higher fracture toughness value. Norton SiC has a G_c value of 88,372 ergs/cm^2, which is consistent.

Carborundum SiC has a much higher grain size, 50 microns, lower density, 2.98 g/cc, and has mostly transgranular fracture, showing cleavage steps and river patterns, and a smoother surface appearance. It has a much lower value of G_c, 60541 ergs/cm^2.

HS-130 Norton and AVCO silicon nitride show intergranular fracture and have a very similar fracture surface appearance. Their densities are almost equal, 3.12 and 3.10 g/cc, respectively. HS-130 Norton Si_3N_4 has a finer grain size (1 micron) than AVCO Si_3N_4 (5 microns), and hence, has a slightly higher value of fracture toughness.

From these observations and discussion it can be said that the denser material with finer grain size which fractures completely intergranularly will have a higher fracture toughness value.

IV. CONCLUSIONS

1. The CMB fracture toughness testing using modified specimens, the jig, and the specimen geometry designed for the application of this technique are suitable for studying slow crack growth in material. Modification to specimen geometry must be carefully considered. If this is done, accurate values of fracture toughness may be obtained.

2. Glass shows slow crack growth at room temperature and the strain energy release rate increases exponentially with the crack velocity.

3. Slow crack growth occurs in plexiglass (PMMA) at room temperature and the stress intensity factor increases with crack velocity.

4. Slow crack growth does not occur in hot pressed silicon nitride and silicon carbide at room temperature. This important finding precludes the use of proof testing to predict lifetime under stress.

5. The strain energy release rate increases with increase in loading rate in the case of both glass and plexiglass, but remains constant with increase in loading rate for silicon nitride and silicon carbide.

6. The denser material with finer grain size which fractures completely intergranularly will have a higher fracture toughness value.

REFERENCES

1. Zaplatynsky, I., "Diffusion of Co^{2+} and Ni^{2+} in MgO," Journal of the American Ceramics Society, 45(1), 28-31 (1962).

2. Wuensch, B. J., and Vasilos, T., "Diffusion of Transition Metal Ions in Single-Crystal MgO," Journal of Chemistry and Physics, 36(11), 2917-22 (1962).

3. Mimkes, J., and Wuttig, M., "Diffusion of Ni^{2+} in MgO," Journal of the American Ceramics Society, 54(1), 65-66 (1971).

4. Wuensch, B. J., and Vasilos, T., "Grain-Boundary Diffusion in MgO," Journal of the American Ceramics Society, 47(2), 63-68 (1964).

5. Nielsen, T. H., and Leipold, M. H., "Hot Pressed High Purity Polycrystalline MgO," Journal of the American Ceramics Society, 48(3), 463-466 (1965).

6. Leipold, M. H., and Kapadia, C. M., "The Effect of Anions on Hot Pressing of MgO," Journal of the American Ceramics Society, 56(4), 200-204 (1973).

7. Blank, S. L., and Pask, J. A., "Diffusion of Iron and Nickel in MgO Single Crystals," Journal of the American Ceramics Society, 52(12) 669-675 (1969).

8. Evans, A. G., and Wiederhorn, S. M., "Crack Propagation and Failure Prediction in Silicon Nitride at Elevated Temperatures," (To be published).

9. Frieman, "Crack Propagation in Ceramics," Report of NRL Progress, February, 1972, pp. 36-38.

10. Charles, R. J., and Hillig, W. B., "Symposium on Mechanical Strength of Glass and Ways of Improving It," Florence, Italy, September 25-29, 1961, pp. 511-527.

11. Marshall, G. P., and Williams, J. G., Journal of Materials Science, 8, (1973), pp. 138-410.

APPENDIX I.

PUBLICATIONS AND PRESENTATIONS

1. "Effect of Anions on Hot-Pressing of MgO," Leipold, M. H., and Kapadia, C. M., Journal of the American Ceramic Society, 56(4) pp. 200-203 (1973).

2. "Correlation of Pore Size and Grain Size During Grain Growth of Oxides," Kapadia, C. M., and Leipold, M. H., Journal of the American Ceramic Society, 56(5) p. 289 (1973).

3. "Grain Growth in Pure Dense MgO," Kapadia, C. M., and Leipold, M. H., Journal of the American Ceramic Society, 57(1), January, 1974.

4. "Grain Boundary Mobility in Anion Doped Magnesium Oxide," Kapadia, C. M., and Leipold, M. H. Accepted for publication in "Proceedings of the Symposium on Surfaces and Interfaces of Glass and Ceramics," Materials Science Research Series, Plenum Press, New York.

5. "The Mechanism of Grain Growth in Ceramics," Kapadia, C. M., and Leipold, M. H. Submitted to the American Ceramic Society Bulletin.

6. "Grain Boundary Mobility in Anion Doped MgO," Kapadia, C. M., Ph.D. dissertation, University of Kentucky, 1974.

7. "Role of Anions in Mechanical Failure - I," Leipold, M. H., and Kapadia, C. M., University of Kentucky, UKY TR25-70-MET12, June, 1970.

8. "Role of Anions in Mechanical Failure - II," Leipold, M. H., and Kapadia, C. M., University of Kentucky, UKY TR42-71-MET14, August, 1971.

9. "Mechanical Behavior of Polycrystalline Ceramics, Brittle Fracture of SiC-Si_3N_4 Materials," Leipold, M. H., Kapadia, C. M., and Kelkar, A. H. Third annual report submitted to the Lewis Research Center, Cleveland, Ohio - September, 1972.

10. "Mechanical Behavior of Polycrystalline Ceramics, Brittle Fracture of SiC-Si_3N_4 Materials," Leipold, M. H., Kapadia, C. M., and Kelkar, A. H. Fourth annual report submitted to the Lewis Research Center, Cleveland, Ohio - September, 1973.

11. "Grain Boundary Microhardness in Anion Doped MgO," presented to National Meeting of American Ceramic Society, Chicago, Illinois, April 28, 1971.

12. "Influence of Anions of Grain Growth in MgO," presented to National Meeting of American Ceramic Society, Chicago, Illinois, April 28, 1971.

13. "Diffusion of Ni^{++} in Anion Doped MgO," presented to American Ceramic Society, Washington, D. C., May, 1972.